Applied Thermal Engineering 160 (2019) 114017

Contents lists available at ScienceDirect

Applied Thermal Engineering

journal homepage: www.elsevier.com/locate/apthermeng

Research Paper

Experimental investigation of a ground-coupled air conditioning system with desiccant assisted enthalpy recovery during winter mode

Peter Niemann*, Gerhard Schmitz

Hamburg University of Technology, Institute of Engineering Thermodynamics, Hamburg, Germany

HIGHLIGHTS

- Desiccant and geothermal assisted air conditioning is promising during winter operation.
- Enthalpy recovery is beneficial against conventional air humidification processes.
- Enthalpy recovery improves highly comfortable indoor air conditions during winter.
- Geothermal system is promising for desiccant assisted air conditioning.
- Using the soil for heating and cooling improves equalizing soil thermal energy balance.

ARTICLE INFO

Keywords:
Air conditioning
Enthalpy recovery
Humidification
Ground-coupled heat pump
System evaluation
Experimental

ABSTRACT

In the framework of a research project at Hamburg University of Technology the combination of an open cycle desiccant assisted air conditioning system and a geothermal system is investigated experimentally by means of a test facility during summer and winter. The system is designed to use a large amount of renewable energies and to reduce electricity demand for air conditioning. Thus, the main objectives of this study are the investigation of the overall system performance and evaluation of geothermal assisted heat supply during winter mode for a temperate climate region, based on measured data. As an important comfort aspect, moisture recovery is considered in detail in terms of coupled heat and mass transfer within the enthalpy wheel; related energy demands are limited to auxiliary energies. Different reference systems are defined to evaluate the performance of the investigated system in terms of energy demand required for air treatment, especially air humidification. The geothermal system is an essential subsystem regarding seasonal storage of thermal energy. Thus, the influence of heat supply using a ground-coupled heat pump on soil temperature development is investigated. Besides system evaluation, measured data regarding thermal comfort are presented.

1. Introduction

Energy efficient air conditioning becomes more and more important due to increasing sales numbers and the resulting energy demand for air conditioning worldwide [1]. The International Energy Agency estimates an increase of more than 5 billion air conditioning systems between the years of 2016 and 2050 for the commercial and residential stock [2]. This is more than a doubling of the currently installed units. Often, air conditioning systems are used to supply cooled and dehumidified air. But from a global perspective final energy demand for space heating is currently still higher than the final energy demand for space cooling applications [3].

Pursuing the goal of reducing the electrical energy demand for air conditioning, desiccant assisted air conditioning systems have been found as promising alternative to conventional air conditioning processes relying on a vapor compression chiller. Thus, a lot of different studies have been undertaken to improve and evaluate desiccant materials as well as different system configurations. Several studies investigated desiccant assisted air conditioning systems during summer mode experimentally or numerically [4–8]. As a specific process layout of desiccant assisted air conditioning, hybrid systems were found to be promising alternative to other air conditioning processes [9]. Even though winter mode is an essential part of full year operation, especially for heating dominated regions, winter mode as well as full year operation of such systems are addressed only in few studies [10–15]. El-Maghlany et al. [10] proposed a two-wheel system with enthalpy and

* Corresponding author.
E-mail addresses: peter.niemann@tuhh.de (P. Niemann), schmitz@tuhh.de (G. Schmitz).

https://doi.org/10.1016/j.applthermaleng.2019.114017
Received 18 April 2019; Received in revised form 6 June 2019; Accepted 24 June 2019
Available online 25 June 2019
1359-4311/ © 2019 The Authors. Published by Elsevier Ltd. This is an open access article under the CC BY-NC-ND license (http://creativecommons.org/licenses/BY-NC-ND/4.0/).

Nomenclature

Symbols

A	area (m^2)
c_p	specific heat capacity ($Jkg^{-1}K^{-1}$)
d	diameter (m)
h	specific enthalpy(Jkg^{-1})
MPF	monthly performance factor (−)
P	electrical power (W)
Q	thermal energy (J)
$\dot{Q}$	thermal power (W)
r	rotational speed (rh^{-1})
r_0	specific evaporation enthalpy (Jkg^{-1})
SPF	seasonal performance factor (−)
$\dot{V}$	volume flow (m^3s^{-1})
W	electrical energy (J)
x	water content ($g_w kg_{air}^{-1}$)
Δ	difference (−)
ϑ	temperature (°C)
λ	thermal conductivity ($Wm^{-1}K^{-1}$)
τ	time (s)
φ	relative humidity (%rh)
Φ	heat recovery efficiency (−)
Ψ	moisture recovery efficiency (−)
$[\cdot\bar{\cdot}\cdot]$	averaged quantity (−)

Subscripts and Abbreviations

AH	air heater
AH-GEO	reference system with adiabatic air humidification and GCHP assisted heat supply
AHU	air handling unit
AUX	auxiliary energies
BHE	borehole heat exchanger
c	conventional
CHP	combined heat and power generation
el	electrical
eha	exhaust air
eta	extract air
EW	enthalpy wheel
EW-GEO	investigated system
GCHP	ground-coupled heat pump
h	heating
HRW	heat recovery wheel
IH-GEO	reference system with isothermal air humidification and GCHP assisted heat supply
in	inlet
m	month
max	maximum
min	minimum
nom	nominal
oda	outside air
out	outlet
p	period
Ref	reference
set	set point temperature
su	summer
sup	supply air
th	thermal
UHS	underfloor heating system
w	water
wi	winter

heat recovery wheel as retrofit solution for an Egypt hospital intensive care unit. Full year system operation is simulated using EnergyPlus™ software. The proposed system shows significant reductions in electricity demand compared to the existing system with electrical heating coil, especially during winter mode. Further investigations on humidification as well as overall system performance during winter operation are not provided. De Antonellis et al. [11] investigated wetting of outside air using a desiccant wheel based on silica gel experimentally and numerically for selected Mediterranean winter conditions. Outside air is dehumidified and humidified regeneration air is supplied to the conditioned space. Thus, the process is relying on active air humidification by making use of a DEC dehumidification process. Experiments were conducted for different cases at steady state. The authors highlight the dependence of air humidification and required regeneration air temperature regarding energy demand and occupants' discomfort for the considered system configuration. Additionally, an energetic performance comparison with conventional humidification technologies like adiabatic, electric steam and steam to steam humidifiers is presented; the overall system is not considered. Simulation results show reduced primary energy demand for air humidification of the proposed system compared to the reference systems with adiabatic and electrical steam humidifiers for different working conditions, whereas primary energy demand of the proposed system was higher compared to reference systems with steam to steam humidifier for the considered boundary conditions. Kawamoto et al. [12] investigated a desiccant assisted system combined with a heat pump for heat supply on the regeneration air side for selected winter days in the east of Japan. The investigated system uses outside air that is dehumidified on one side and remoistened on the other side of a desiccant wheel. It is shown that for this kind of active humidification, humidification rate is increased with increasing regeneration air temperature or volume flow rate of process air. La et al. [13] examined a system configuration with solar thermal heat supply and one-rotor two-stage desiccant wheel during winter in Shanghai. Extract air from the conditioned space is used to humidify supply air. The study shows a significant increase in thermal comfort for different winter days and draw attention to the space requirements for solar collectors to improve thermal comfort. Additionally, the study of Li et al. [14] shows experimental results for the same system for summer and winter operation. The authors focus on performance of solar assisted heat supply during winter in terms thermal indoor air comfort, whereas desiccant assisted air humidification is not considered. In Preisler and Brychta [15] full year operation of a desiccant assisted evaporative system is investigated experimentally in Austria. During full year operation, a reduction of primary energy demand of 60% is achieved in comparison to a reference system relying on a vapor compression chiller. The authors outline the high energy saving potentials of the investigated system, whereas details about the humidification process and the reference system are not provided.

Dry air conditions in air conditioned buildings without additional humidification systems can adversely affect occupants' comfort, especially in modern buildings relying on mechanical ventilation during winter. Zhao et al. [16] analyzed the effects of mechanical and natural ventilation in residential buildings for the period of one year experimentally. The authors found lower indoor air humidity levels for the mechanical ventilated residential buildings during the investigated winter period. Adverse effects on human comfort and health related to dry air conditions have been addressed in many studies [17–20]. Wolkoff [21] reviewed literature to deeply investigate the dependencies of human health and humidity level. The effect of low humidity level on perceived temperature and skin characteristics in terms of skin's shrinking is investigated by Berglund [22]. The author found that

comfort limitations due to dry nose, throat, eyes and skin increase at low humidity. The same holds true for respiratory illness and absenteeism. Reinikainen et al. [23] present the results of a field study to analyze the effects of air humidification for office workers. They found increased occupants' sensation when indoor air is humidified to $\varphi = 30\cdots40\%$rh during office hours. Additionally, proper functioning air conditioning equipment is required to avoid adverse health effects of air humidification. Reinikainen and Jaakola [24] conclude within their study that appropriate air humidification alleviates dry air related health symptoms during heating period. Regarding isothermal air humidification the authors note the risk of stuffy air.

Within a desiccant assisted system, moisture recovery by means of the existing hygroscopic materials is possible. A hygienic advantage of desiccant assisted moisture recovery against conventional air conditioning relying on adiabatic or isothermal air humidification is the fact that no liquid or vaporous water is sprayed into the process air stream.

To the best of the authors' knowledge there is no study investigating winter operation of an air conditioning system relying on enthalpy wheel and ground-coupled heat pump for temperate, heating dominated climate conditions. Few studies investigated air humidification using active humidification with a desiccant wheel. Literature lacks of investigations considering longer periods during winter. Furthermore, in most cases a holistic consideration of the overall system is not addressed, including heat supply and subsystems. In [7,8] the considered system is evaluated in summer mode, using a borehole heat exchanger (BHE) for cooling applications. The system is verified to be a promising alternative compared to conventional air conditioning systems in temperate climate regions. Furthermore, Speerforck et al. [25] proved applicability of the proposed system at different investigated locations by means of a system model using modeling language Modelica®. The authors investigated one cooling period, whereas winter mode is not observed.

Within this study the geothermal and desiccant assisted system is investigated experimentally for a three-month winter period. Moisture recovery is achieved by an enthalpy wheel, passive humidification, to improve indoor air conditions; sensible heat loads are primarily covered by underfloor heating. In combination with a geothermal system, temperature level of underfloor heating enables efficient operation of a ground-coupled heat pump. The performance and limitations of the investigated system are analyzed. Especially, performance of the enthalpy wheel and the geothermal system are addressed. Additionally, the system is compared to reference systems with electric isothermal or adiabatic humidification to investigate to what extent the investigated system is beneficial against other air conditioning processes in winter operation.

2. Test facility

The test facility, located on the campus of Hamburg University of Technology, and its main components in terms of winter operation are shown in Fig. 1. In total, the test facility consists of eight 20 ft. containers. The four containers on the lower floor accommodate the air handling unit as well as further technical installations. The upper four containers serve as office and conference room which is used as reference room for the air conditioning system.

2.1. System layout

As shown in Fig. 2, the schematic layout can be divided into three subsystems: the air handling unit, the reference room and the hot and cold water circuit. Designed as a hybrid system, the test facility combines an open desiccant assisted humidification process with a closed heating loop.

In the following, plant operation in winter mode is carried out. First, outside air (oda) is passing an enthalpy wheel on the process air side ($1 \rightarrow 2$). Thus, outside air is remoistened and reheated within this process using the extract air stream. If necessary, humidified and/or preheated air is finally heated to the desired supply air (sup) temperature in a sensible water to air heat exchanger ($3 \rightarrow 4$), before it is supplied to the conditioned space. In this case, the heat recovery wheel (HRW) is not operated. The resulting air path is shown with the dark gray path in Fig. 2. If outside air humidity is within comfort limits regarding water content, it is preheated using a heat recovery wheel ($2 \rightarrow 3$). In this case the enthalpy wheel is bypassed (light gray air path according to Fig. 2). Extract air (eta) from the conditioned space is used for sensible heat recovery ($5 \rightarrow 6$) or coupled sensible and latent heat recovery ($7 \rightarrow 8$), according to the air handling process as described above. In case of very low outside air temperatures, a water to air heat exchanger ($6 \rightarrow 7$) can be operated to avoid condensation of water vapor within the enthalpy wheel. Air pressure loss across relevant AHU components and characteristics of the wheels are listed in Table 1. In contrast to a conventional air conditioning system, moisture recovery using the existing hygroscopic material for the dehumidification process during summer mode is possible. Additional technical equipment in terms of an isothermal or adiabatic air humidifier is not required. Therefore, the related energy demand is limited to auxiliary energies.

Bypassing the enthalpy wheel for demand-oriented air humidification reduces the electrical energy demand of the fans. Cooling and dehumidification of process air is not provided during winter operation. The reference room is connected to the air handling unit on the supply and extract air side. Additionally, to cover sensible heat loads directly, the reference room is equipped with underfloor heating.

Generally, desiccant assisted air conditioning enables the integration of heat sinks operating on temperature levels above dew point temperature, e. g. shallow geothermal energy, during summer mode. Utilizing the geothermal system during full year operation as heat sink and heat source is promising for the reason of improving the annual thermal energy balance of the soil. Thus, thermal energy in form of heat required for heat supply is primarily provided by a ground-coupled heat pump (nominal thermal power output: $\dot{Q}_{GCHP,nom} = 5.1 kW_{th}$ at BW5/W30). A small scale gas driven CHP unit (nominal thermal power output: $\dot{Q}_{CHP,nom} = 12.5\ kW_{th}$, nominal electrical power output: $P_{CHP,nom} = 5 kW_{el}$) is utilized as backup system and for covering thermal peak loads. As a solar thermal system with flat plate collectors ($A_{STU} = 20 m^2$) is integrated in the hot water circuit as primary heat source for summer mode, solar thermal energy is utilized as subordinated heat source during winter mode as well. Integrating a

Fig. 1. Test facility, air handling unit and heat pump.

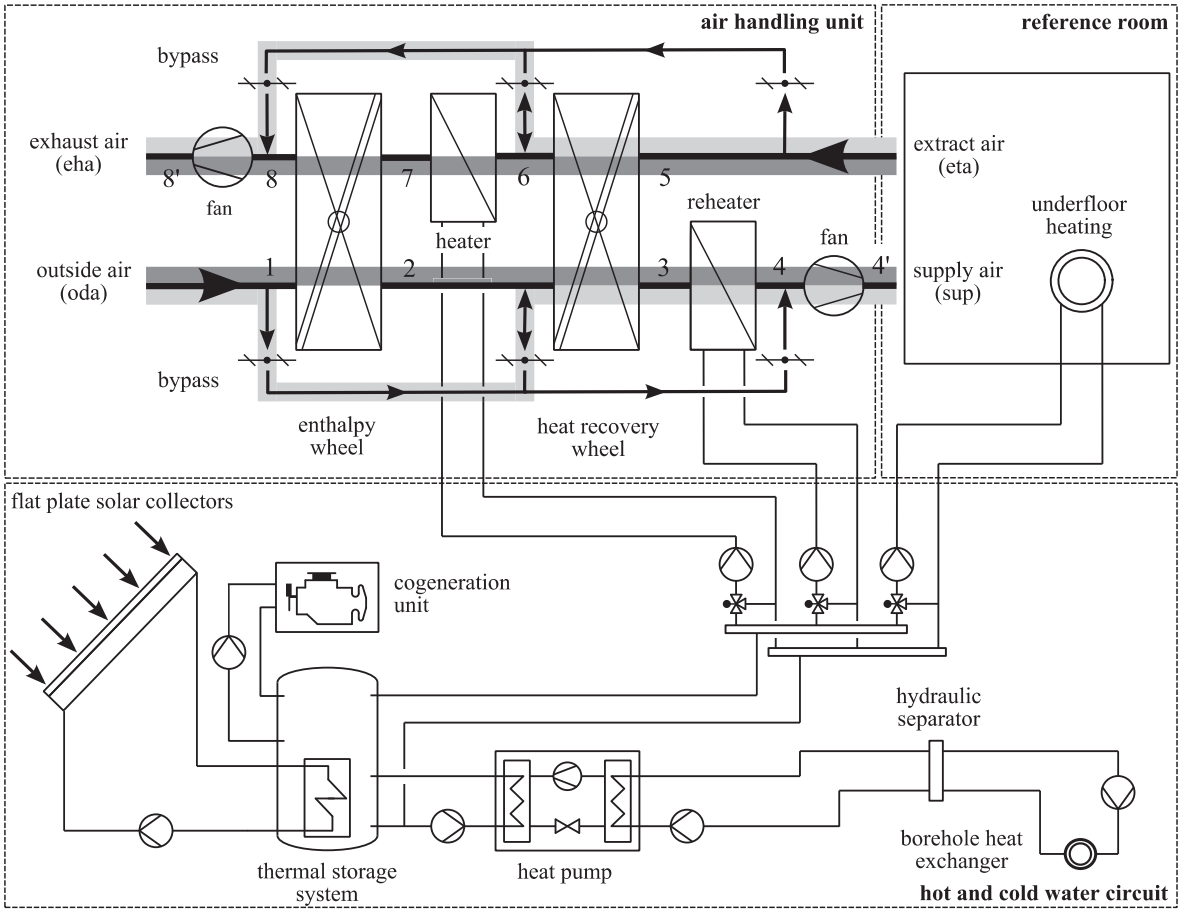

Fig. 2. System layout of the test facility.

Table 1
Parameters and characteristics of specific AHU components.

Air pressure loss of specific components in Pa		Characteristics of the wheels	
EW	180 ± 6	Desiccant material	LiCl
HRW	104 ± 6	Diameter	0.6 m
Heater/reheater	17 ± 6	Rotational speed	248 rh^{-1}

stratified thermal storage system of 1 m^3 within the hot water circuit enables heat supply and heat demand to be decoupled timewise. A mixture of water and 22% ethylene glycol is used as heat transfer fluid within the hot and cold water circuit. Fig. 3 includes information about electrical power demands of the system at nominal operation separated according to relevant components.

As shown in Fig. 4, the geothermal system consists of one double U-tube borehole heat exchanger (BHE), supplying the ground-coupled heat pump (GCHP) unit. A reference BHE is used to analyze the impact of geothermal energy supply on soil temperature in the surrounding soil. The reference BHE is not in use for thermal energy transfer; solely its thermistor string is utilized for evaluation in this case.

The soil primarily consists of fine, medium and coarse sand up to a depth of 18 m below ground surface. Below this, a layer of till and silt is located. For the remaining length below 30 m the BHE is surrounded by micaceous clay. The final drilling depth of the BHE is 80 m below ground surface. Significant ground water flows do not occur at the drilling location in general, utilizing the soil as seasonal thermal storage. A grouting material with a thermal conductivity of $\lambda = 2$ $Wm^{-1}K^{-1}$ is used for thermal connection between BHE ducting and surrounding soil.

2.2. Data acquisition

Air temperature and relative humidity are measured at the inlet and outlet of each component within the air handling unit. Labeling of each air state is shown in Fig. 2. Installed sensors measuring relative humidity are designed as combined sensors with additional integrated Pt100 resistance thermometers. Flow averaging is applied as proposed by Slayzak and Ryan [26] to take into account inhomogeneity within the air streams, especially behind rotating components. Air side pressure drop across each component is acquired. Volume flows of supply and extract air are measured at position 4 and 8, according the principle of differential pressure. Each hydraulic circuit is evaluated by measurement of volume flow and fluid temperature at the inlet and outlet of each component. With respect to Fig. 4, thermistor strings are integrated in the borehole heat exchangers next to the BHE ducting for temperature measurements in different depths below ground surface (10, 15, 20, 40, 60 and 80 m). Electrical energy demand of each component (e. g. heat pump, fans and circulation pumps) is measured as well as further relevant parameters characterizing thermal comfort (e. g. globe temperature and air velocity) within the reference room.

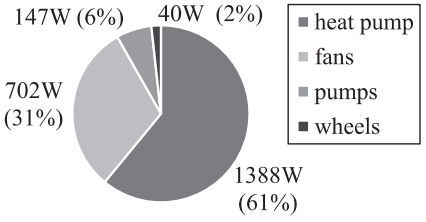

Fig. 3. Electrical power demands.

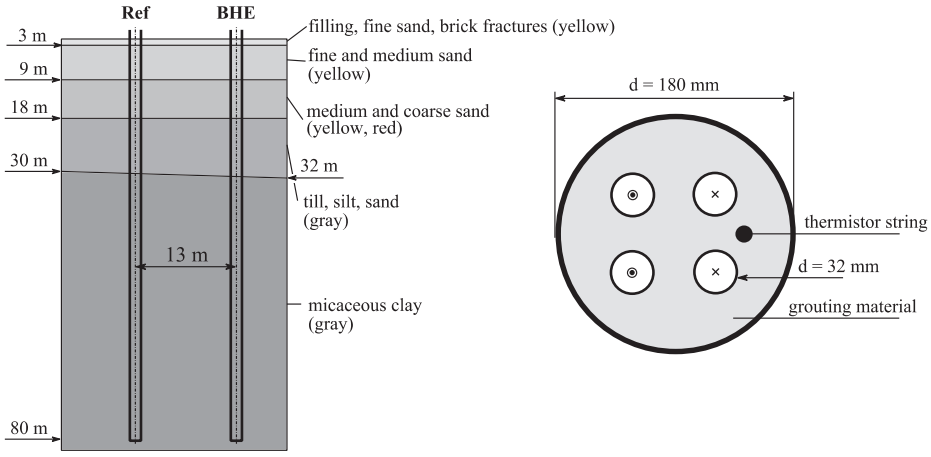

Fig. 4. Structure of the soil and layout of the borehole heat exchangers.

Summarizing, measurement devices in use and related uncertainties are listed in Table 2. All measurement signals are recorded once per minute. A National Instruments data acquisition system and corresponding LabVIEW software in connection with Siemens S7 controlling is used to control and to regulate the overall system.

3. Measurement results

Experimental results presented below are based on measurement data from the heating period in 2017 for the months of January till March. The test facility is operated from 7 am to 10 pm every day of the week. First, the investigated system is evaluated with regard to steady state operation and performance of moisture recovery and indoor air conditions. Subsequently, the system is compared with two reference systems relying on electric isothermal and adiabatic humidification regarding total electrical and thermal energy demands. Finally, the performance of the geothermal system is evaluated.

3.1. System performance

The stationary operation state considered in the following was recorded on a representative cold winter day in northern Germany. Fig. 5(a) shows the state changes of air during the air conditioning process in a h, x-diagram according to Mollier. The state changes (dark grey lines) are marked according to the numbering in Fig. 2. Since there are almost no state changes within the fans, the corresponding air conditions downstream of the fans (4′, 8′) are not plotted. Volume flows of supply and extract air are controlled to be equal in the range of $(950 \pm 95)\mathrm{m^3h^{-1}}$. The heater on the extract air side was not in use for the entire period. Additionally, equivalent state changes of process air for a reference system relying on isothermal humidification (dashed grey lines) are shown for process comparison as well. The underlying layout of the air handling unit is shown in Fig. 5(b). The corresponding air states are marked by subscript "c".

Comparing the process-specific state changes shows the differences between both processes. For the desiccant assisted system water content of process air is increased by enthalpy recovery ($1 \rightarrow 2$) from extracted room air, whereas humidification in the reference process is achieved by a steam humidifier ($2_c \rightarrow 3_c$). Before humidification, outside air is preheated by a regenerative heat exchanger ($1_c \rightarrow 2_c$). For both processes supply air temperature is adjusted within the reheater ($3 \rightarrow 4$, $3_c \rightarrow 4_c$). The hardly visible difference between air state 2 and 3 in Fig. 5(a) is caused by measurement uncertainties. The quality of the desiccant assisted process can be evaluated by means of energy and mass balance for the enthalpy wheel. It is noticeable that the enthalpy difference on the process air side is reduced by 13.3% with respect to extract air side. The resulting state changes on both sides of the enthalpy wheel run not ideally in parallel, see Fig. 5(a). One reason for this are air conditions outside the calibrated area of the measurement devices in use, affecting air stage 1 and 8 with resulting higher uncertainties of these air states. This limits the total energy balance of the air handling unit significantly. A similar characteristic holds true for the moisture mass balance of the air handling unit. Average values for total energy balance and moisture mass balance are listed in Table 3 for steady state operation of the system. Values are taken into account for steady state if sup water content is changing less than $0.5\mathrm{g_w kg_{air}^{-1}}$ and fluctuation of eta temperature is less than 0.5K within 15 minutes.

During the entire period, rotational speed of EW and HRW was kept constant. In previous investigations the optimal rotational speed of the EW regarding moisture and heat recovery efficiency was found to be at $248\ \mathrm{rh}^{-1}$. Both, average moisture and heat recovery efficiency are $\Psi_{EW} = \Phi_{EW} \approx 0.75$. Average heat recovery efficiency of the HRW is $\Phi_{HRW} = 0.61$ at $248\ \mathrm{rh}^{-1}$.

The internal latent loads within the reference room were almost constant at $0.61\mathrm{kg_w h^{-1}}$ on weekdays and $0.38\mathrm{kg_w h^{-1}}$ at the weekends. In the following, moisture recovery is considered in more detail. Fig. 6 shows the resulting moisture recovery efficiency (a) and total moisture recovery (b) depending on the moisture potential ($\Delta x_{max} = x_7 - x_1$, according to Fig. 2).

Moisture recovery efficiency as shown in Fig. 6(a) is defined as

Table 2
Measurement devices used and related measurement uncertainties.

Measured value		Sensor type/measuring principle	Measurement uncertainty
Air and water temperature	ϑ	Pt100 (accuracy class W 0.1)	$\pm 1/3{\cdot}(0.3 + 0.005{\cdot}\vartheta)$K
Soil temperature	ϑ	Thermistor string	± 0.5K
Relative humidity	φ	Capacitive humidity sensor	± 2% rh for 10⋯90%rh
Volume flow (air)	$\dot{V}$	Differential pressure	± 10% of reading
Volume flow (water)	$\dot{V}$	Electromagnetic flow meter	± 0.5% ± $1\mathrm{mms^{-1}}$ of reading
Pressure difference	Δp	Ceramic fulcrum lever technology	± 2% of full scale (range: 0⋯300Pa and 0⋯1000Pa)
Electric power	P	AC energy meter	± 2% of reading

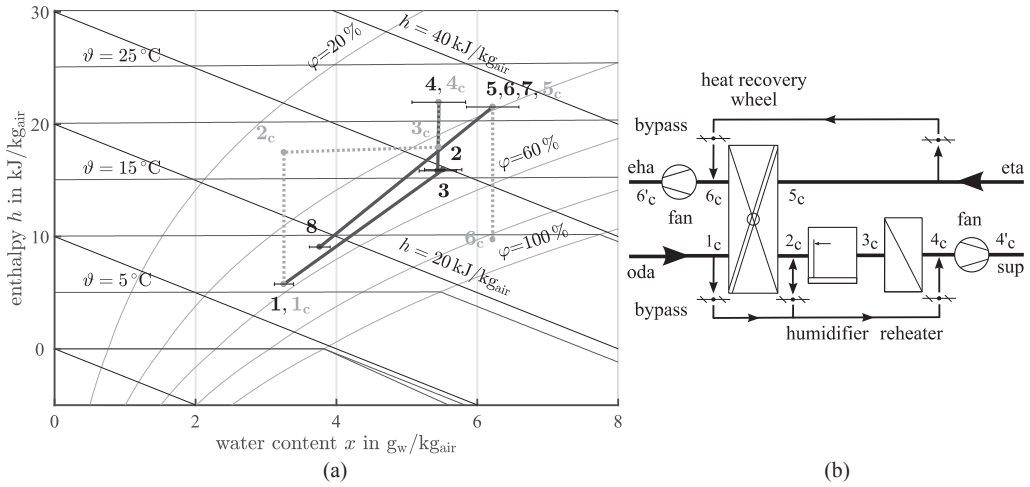

Fig. 5. State changes of air in the air conditioning process (a) and air handling unit of the reference system (b).

Table 3
Average values of total energy balance and moisture mass balance.

	Total Energy Balance	Moisture Mass Balance
Air handling unit	0.90 ± 0.03	0.96 ± 0.03
Enthalpy wheel	0.94 ± 0.03	1.00 ± 0.03
Heat recovery wheel	0.93 ± 0.02	1.00 ± 0.03

$$\Psi = \frac{x_{\mathrm{sup}} - x_{\mathrm{oda}}}{x_{\mathrm{eta}} - x_{\mathrm{oda}}} = \frac{x_2 - x_1}{x_7 - x_1} \tag{1}$$

with respect to the numbering in Fig. 2. Regarding the range of moisture potential, an increasing moisture recovery potential is visible. The slope of the resulting linear trend curve is $\Delta\Psi = 0.04 \cdot (\mathrm{g_w kg_{air}^{-1}})^{-1}$, representing a low dependence of Ψ on the available moisture potential. Around 90% of the operating points are located in the range of $1 \cdots 2 \mathrm{g_w kg_{air}^{-1}}$. The average moisture potential is $1.49 \mathrm{g_w kg_{air}^{-1}}$. In combination with the corresponding moisture recovery efficiency, water content of process air is increased by $1.1 \mathrm{g_w kg_{air}^{-1}}$, enhancing comfort conditions in the reference room. Caused by low dependence of Ψ on moisture potential, the total moisture recovery can be described in a good approximation as a linear function of Δx_{max} with narrow fluctuation margin, see Fig. 6(b). The maximum deviation from the resulting trend curve is $0.21 \mathrm{g_w kg_{air}^{-1}}$. These fluctuations appear stronger in relation to moisture recovery efficiency, caused by the definition of Ψ as shown in Eq. (1) and the occurring small range of values. Regarding the overall enthalpy exchange in the EW by separating energy exchange in form of heat divided into sensible and latent heat exchange, the average share of sensible heat exchange is 81% and 19% for latent heat exchange, respectively. Thus, enthalpy exchange using an EW based on LiCl includes primarily sensible heat exchange under the given boundary conditions.

De Antonellis et al. [27] proposed correlations of sensible and latent effectiveness for enthalpy wheels. The effectiveness parameters are defined as shown in Eqs. (2) and (3). Used indices refer to the inlet and outlet positions of the considered components.

$$\eta_{\mathrm{sen}} = \frac{|\dot{m}_{\mathrm{air,sup}} \cdot \bar{c}_{p,\mathrm{sup}} \cdot (\vartheta_{\mathrm{out,sup}} - \vartheta_{\mathrm{in,sup}})| + |\dot{m}_{\mathrm{air,eta}} \cdot \bar{c}_{p,\mathrm{eta}} \cdot (\vartheta_{\mathrm{out,eta}} - \vartheta_{\mathrm{in,eta}})|}{2 \cdot (\dot{m}_{\mathrm{air}} \cdot \bar{c}_p)_{\mathrm{min}} \cdot (\vartheta_{\mathrm{in,eta}} - \vartheta_{\mathrm{in,sup}})} \tag{2}$$

$$\eta_{\mathrm{lat}} = \frac{|\dot{m}_{\mathrm{air,sup}} \cdot r_0 \cdot (x_{\mathrm{out,sup}} - x_{\mathrm{in,sup}})| + |\dot{m}_{\mathrm{air,eta}} \cdot r_0 \cdot (x_{\mathrm{out,eta}} - x_{\mathrm{in,eta}})|}{2 \cdot (\dot{m}_{\mathrm{air}} \cdot r_0)_{\mathrm{min}} \cdot (x_{\mathrm{in,eta}} - x_{\mathrm{in,sup}})} \tag{3}$$

Fig. 7 shows the effectiveness parameters for measured stationary operating states in dependence of the underlying energy transfer potential regarding EW and HRW. All effectiveness parameters show almost constant dependencies with narrow fluctuation for the given ranges of transfer potential. Thereby, the averaged effectiveness parameters of the enthalpy wheel $\eta_{\mathrm{EW,lat}} = \eta_{\mathrm{EW,sen}} \approx 0.80$ are slightly higher than the averaged sensible effectiveness of the heat recovery wheel $\eta_{\mathrm{HRW}} = 0.73$. Besides material-specific heat transfer properties, the effectiveness parameters are primarily limited by air leakage at the rotating components in this case. These air leakages are mostly driven by

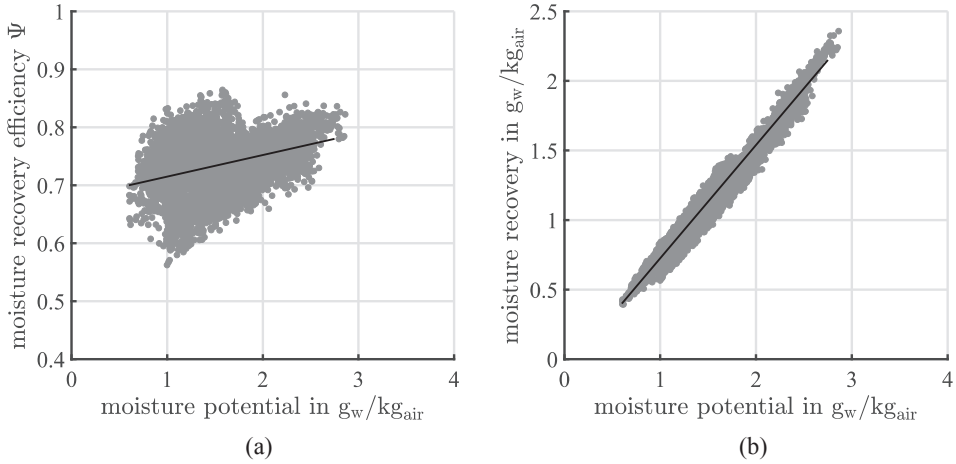

Fig. 6. Performance of moisture recovery by means of moisture recovery efficiency (a) and total moisture recovery (b).

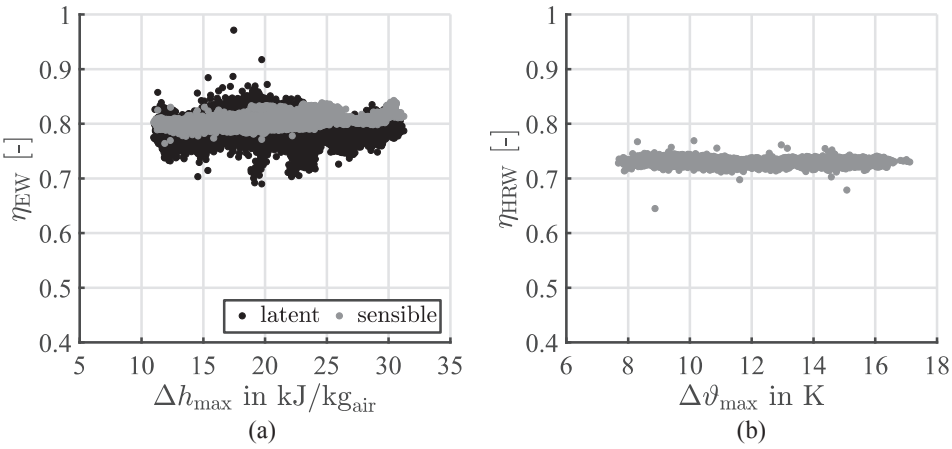

Fig. 7. Latent and sensible effectiveness for the enthalpy wheel (a) and sensible effectiveness for the heat recovery wheel (b).

pressure differences between the channels of supply and extract air. Due to different boundary conditions regarding desiccant material, rotational speed and temperature inlet conditions, a direct comparison to the results of De Antonellis et al. is not possible. Nevertheless, the obtained results in this study show good efficiency of the wheels, especially for heat and mass recovery at the enthalpy wheel.

These characteristics are important regarding the resulting indoor air conditions. Referring to this, Fig. 8(a) shows outside and room air conditions during plant operation for the investigated period with simplified comfort areas category I and II according to DIN EN 15251 [28]. In order to exclude start-up effects, the first hour of system operation is not considered. Compared with the annual average number of ice days for preceding decades (16.4 ice days for the years 1981–2010), provided by the German Meteorological Service, the investigated period is classified as moderate winter period (5 ice days). The comfort areas are defined to ensure less than 6% (cat. I) and 10% (cat. II) of occupants being dissatisfied with the present indoor air conditions. In total, 99.7% of outside air conditions were outside comfort area according to cat. I and 99.5% according to cat. II, respectively. Days within the comfort area occurred during the period at the end of March. The average outside air temperature in January was 1.67 °C at an average water content of $3.3 g_w kg_{air}^{-1}$. The other months are characterized by higher temperature and water content of outside air. Without humidification of supply air, over 60% of room air conditions would be outside of cat. I. During system operation, around 67% of room air conditions satisfied the requirements according to cat. I and cat. II is maintained for 75% of system operation, respectively. These deviations from ideal indoor air conditions were primarily caused by indoor air temperatures below 21 °C (cat. I) or 20 °C (cat. II). 85% of these indoor air conditions occurred during the first four hours of daily plant operation, caused by lower internal sensible loads and the control strategy of underfloor heating. Similar characteristics hold true for water content of indoor air. With respect to comfort requirements according to cat. I, 20% of indoor air conditions are characterized by too low water content, occurring for 55% within the first four hours of daily plant operation. The system was not capable of providing comfortable indoor air conditions according to cat. I for 75% when water content of outside air was below $2.5 g_w kg_{air}^{-1}$. Over-humidification of room air did not occur during the entire period.

The operation strategy of the underfloor heating system (UHS) is relying on the current outside air temperature with underlying heating curve. With respect to Fig. 8(b), a trend of increasing fluctuation of indoor air temperature with increasing inlet temperature of the underfloor heating system is noticable. Operating states with lower indoor air temperatures than the set point temperature ($\vartheta_{room,set}$ = 22°C) at UHS inlet temperatures above 35 °C were just occurring during the first hours after system start-up, limiting thermal comfort in the morning as mentioned above. The relationship presented in Fig. 8(b) shows improvement potential for the control strategy of the underfloor heating system. Similar to a kind of night setback, the underfloor heating system was operated during night, while the central thermal storage system was not loaded between 10 pm and 7 am for this study. At the same time the GCHP was not operated, respectively. To avoid low indoor air temperatures in the morning, start-up of the heat supplying subsystems has to be earlier before regular office hours as defined above. Operating the GCHP during night would increase temperature level of the thermal storage system. Additional required electrical energy to run the GCHP is expected to be lower compared to the

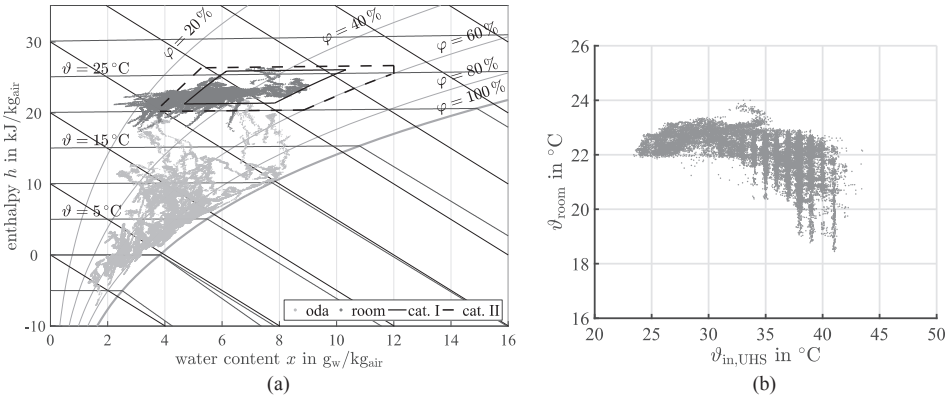

Fig. 8. Outside and room air conditions during plant operation for the investigated period (a) and relationship between room air temperature and underfloor heating inlet temperature (b).

equivalent energy demand during daytime. This is an effect of increased performance as a result of lower required temperature lift.

With the given outside air conditions and the implemented control strategy, the system was operated in EW mode for more than 70% of operation time, respectively 30% of operation time are operated with sensible heat recovery.

3.2. System comparison

To further evaluate the presented system regarding electrical and thermal energy demands, especially in terms of the humidification process, it is compared with two reference systems relying on adiabatic or isothermal humidification. Fig. 5(b) shows the corresponding layout of the air handling unit. Characteristics and assumptions of the numerical models are described in the following. The first reference system (AH-GEO) is relying on adiabatic humidification using an electrical powered impeller humidifier and the second reference system (IH-GEO) is equipped with isothermal humidification relying on an electrical powered steam humidifier. Both humidifiers are designed to ensure the same increase in water content of supply air as the enthalpy wheel of the investigated system (EW-GEO); operation time is based on EW mode. Both reference systems rely on heat supply as the presented system. Energy in form of heat is primarily supplied by a heat pump accordingly. Heat demands of the reheating coil are adapted to the process specific requirements. The lower total pressure loss resulting from non-existent enthalpy wheel is taken into account and leads to reduced electrical energy demand of the fans. A constant heat recovery efficiency for the HRW of 0.75 is assumed. Further process characteristics comply with the investigated system.

Fig. 9 shows the results of the system comparison for the overall period from January to March. Electrical and thermal energy demands are evaluated separately.

Electricity demand of the heat pump and corresponding auxiliary energies are listed under the category “supply”. Heading “ventilation and distribution” includes electricity demand of the air handling unit and circulation pumps of the hydraulic circuits for energy distribution. Focusing air humidification, the corresponding electricity demand is listed separately in Fig. 9(a). The electricity demand for air humidification of the reference system IH-GEO is increased by a factor of 18.0 compared to the investigated system EW-GEO. Thus, the energy demand associated with the electrical steam humidifier is as high as the electrical energy demand for ventilation and distribution, whereas the electrical energy demand of enthalpy wheel is only 4% of the corresponding electricity demand for the air handling unit. Regarding the system AH-GEO, the electricity demand for air humidification is reduced by 62% compared to the investigated system due to the reduced electricity demand of the fans and low additional electricity demand for the circulation pump of the adiabatic humidifier. For all systems the electricity demand for ventilation and distribution is primarily caused by the fans with over 90%. Due to substitution of required thermal energy for reheating by isothermal humidification (IH-GEO), the resulting electricity demand to operate the GCHP is reduced by 23% compared to the other systems (EW-GEO, AH-GEO). In total, the electricity demand of the investigated system is reduced by 18% compared to the system IH-GEO; it is increased by 7% against the system AH-GEO.

Thermal energy demands to operate underfloor heating are equated for the different systems. As mentioned before, thermal energy required for heating of process air to the desired supply air temperature is substituted by the steam humidifier (IH-GEO). Therefore, the thermal energy demand for reheating within the other systems (EW-GEO, AH-GEO) is about 44% higher. Regarding this, the electricity demand of the heat pump and the thermal energy demand of the system AH-GEO is slightly higher compared to the investigated system (EW-GEO), caused by the slight temperature decrease due to injection of cold water.

The system comparison shows lowest electricity demand for the reference system AH-GEO. Thus, it has a slight advantage against the investigated system for the considered period. Electricity demand for the injection of water is nearly as high as the additional required electricity demand of the fans to overcome the pressure loss across the enthalpy wheel. At the same time, thermal energy demand of these two systems (EW-GEO, AH-GEO) is in the same range. Therefore, the investigated system is not unlimited beneficial from an energetic point of view for the considered period. But on the other hand, moisture recovery using an enthalpy wheel is beneficial against the reference technologies regarding hygienic aspects, especially for the use of LiCl as desiccant material. Emission of bacteria caused by air humidifiers as for example described by Strindehag and Josefsson [29] is avoided.

3.3. Geothermal system

The soil temperature 15 m below ground surface is found to be independent of seasonal related temperature fluctuations. With regard to Fig. 4, Fig. 10(a) shows the temperature profile of the BHE in use (gray line) and the reference BHE (dashed black line) for the period of one year including summer and winter mode. The curves result from averaging measured temperatures below 15 m for each BHE. Decreasing temperature level until mid of February is caused by continuous energy extraction in form of heat when the GCHP was operated. The lowest temperature was 4.5 °C. Starting from this point, the soil temperature increased until the end of the investigated period, reaching the temperature level of the reference BHE at the end of March. Balancing winter and summer operation in combination with natural

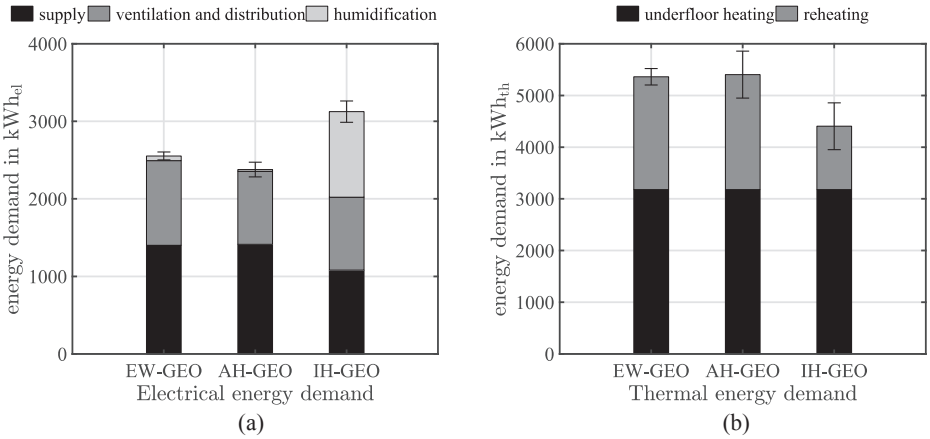

Fig. 9. Electrical (a) and thermal (b) energy demands of the investigated system (EW-GEO) and reference systems (AH-GEO, IH-GEO) for the entire period under consideration (January to March).

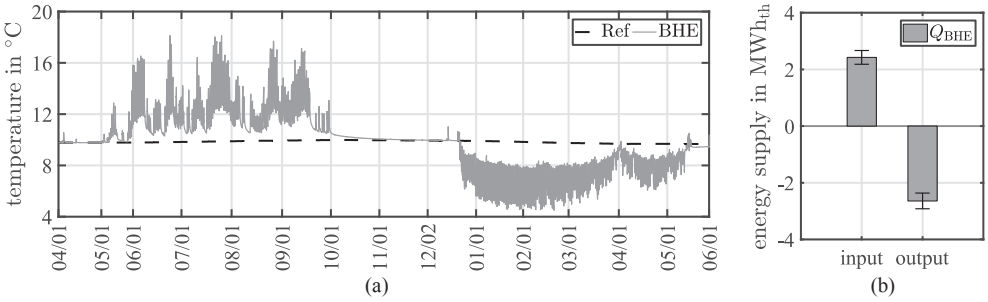

Fig. 10. Temperature profile for the BHE and reference BHE (a) and annual energy balance of the soil (b).

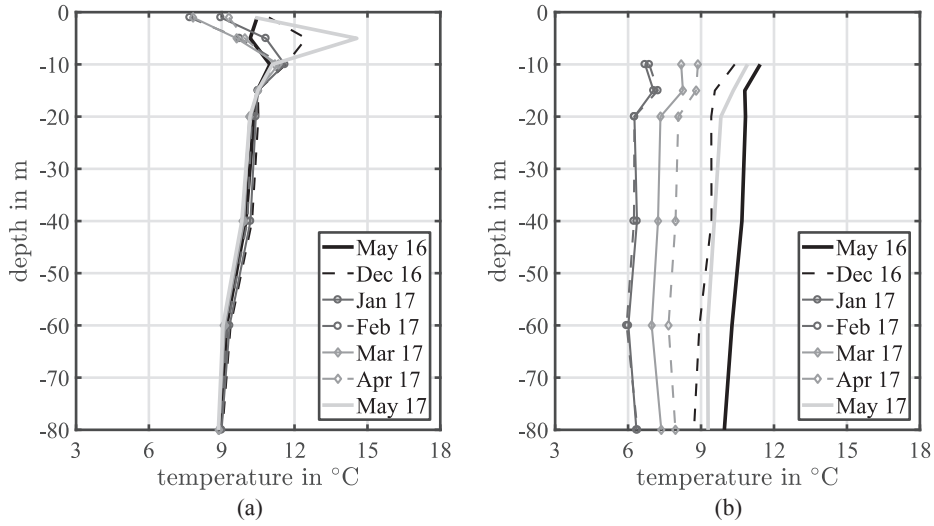

Fig. 11. Temperature profiles depending on drilling depth of the reference BHE (a) and the BHE in use (b).

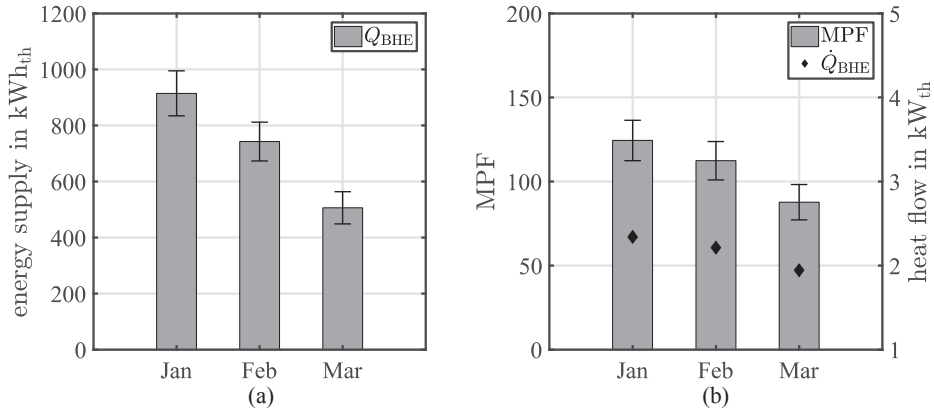

Fig. 12. Energy transferred from the soil (a) and performance of the BHE (b).

regeneration, an equalized energy balance of the soil is achieved. The input and output of thermal energy at the BHE is balanced with a remaining annual difference of 0.22MWh$_{th}$, 9% respectively, as shown in Fig. 10(b). This difference is within the measurement uncertainty of the corresponding energy values. The temperature of the undisturbed soil was 10 °C before winter operation of the test facility. There seems to be a slight influence on the soil temperature around the reference BHE caused by using the soil as heat source, which is hardly visible in Fig. 10(a). The minimum temperature of 9.7 °C was achieved right at the beginning of summer operation. But with respect to the measurement devices used, the occurring temperature difference is still within the corresponding range of measurement uncertainty.

In addition to Fig. 10, depth dependence of temperature profiles is shown in Fig. 11 for the reference BHE (a) and the BHE in use (b), respectively. The characteristics of the curves show monthly average temperatures for each measuring point of the corresponding thermistor string. Below a drilling depth of 10 m, temperature profiles of the reference BHE are very similar for the period under consideration. Between 20 m and 60 m below ground surface soil temperature decreased from 10.5 °C to its lowest value of approx. 9 °C. In spite of shallow environmental influences with seasonal fluctuation, the soil surrounding the reference BHE was not influenced by utilizing geothermal energy at the drilling location in general. Using the soil as heat source surrounding the BHE in use induced decreasing temperature over the considered winter period. Taking the initial situation in May 2016, all monthly averaged temperature profiles were located at lower soil

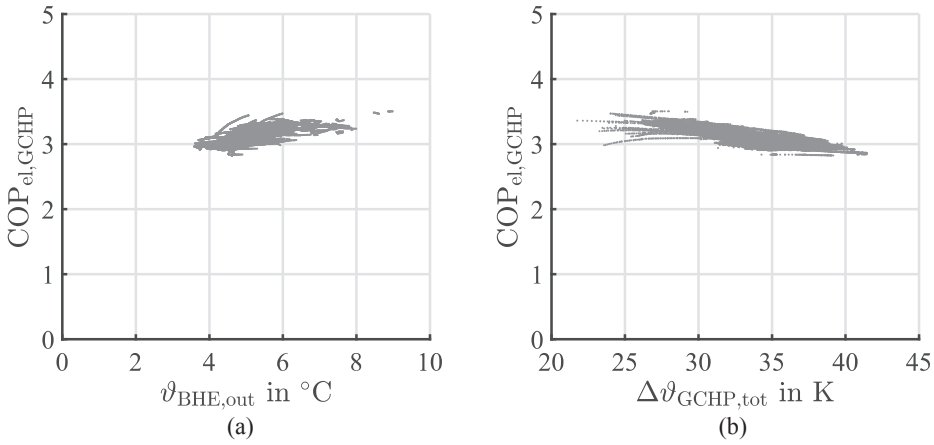

Fig. 13. GCHP electrical COP depending on BHE outlet temperature $\vartheta_{BHE,out}$ (a) and total temperature lift $\Delta\vartheta_{GCHP,tot}$ (b).

temperatures until the beginning of the following cooling period. For all months the temperature profiles were constant in good approximation below a drilling depth of 20 m. For this reason the geothermal system was used equally over the complete drilling depth.

Even though the geothermal system is only utilizable for heat supply in conjunction with a ground-coupled heat pump, both systems, BHE and GCHP, are evaluated separately for the following reasons. First, performance limitations can be assigned to the subsystems and second, a direct comparison with summer mode is possible. Fig. 12 shows the energy transferred from the soil per month (a) and performance indicators of the BHE (b).

The energetic evaluation of the BHE is based on key figures as defined by Speerforck and Schmitz (2016), relating transferred thermal energy with the electrical energy demand of the circulation pump.

$$\mathrm{MPF} = \frac{\int_m \dot{Q}_{BHE}\,d\tau}{\int_m P_{el}\,d\tau},\ \mathrm{SPF} = \frac{\int_p \dot{Q}_{BHE}\,d\tau}{\int_p P_{el}\,d\tau} \tag{4}$$

Monthly Performance Factors are in the range of MPF = 124 ± 12 in January to MPF = 89 ± 10 in March. Decreasing performance over the period is caused by decreasing heat flow as a result of decreasing average temperature level of the soil around the BHE. The resulting SPF is SPF_{wi} = 110 ± 11, indicating a high efficiency of the geothermal heat source. The electrical SPF of the ground-coupled heat pump ($SPF_{GCHP} = Q_h/W_{el}$) is SPF_{GCHP} = 3, limiting the capacity of the geothermal assisted heat supply.

To further analyze the performance of the GCHP, its electrical COP is evaluated for different boundary conditions as shown in Fig. 13.

As shown in Fig. 13(a), BHE outlet temperatures are mostly pooled in the range of $\vartheta_{BHE,out}$ = 3.8...8 °C. Increasing values of $\vartheta_{BHE,out}$ correlate with decreasing load of the geothermal assisted heat supply or sufficient regeneration time for the soil and result in better GCHP performance. Maximum GCHP performance at steady state is $COP_{el,GCHP}$ = 3.5. With respect to Fig. 13(b), GCHP performance is also slightly depending on GCHP load. Here, GCHP load is represented by the temperature difference $\Delta\vartheta_{GCHP,tot}$ between inlet temperature at the evaporator and outlet temperature at the condenser. The amount of operating states at $COP_{el,GCHP} < 3$ increase with increasing load above 32 °C to supply the underfloor heating system. Generally, performance of the investigated GCHP system is not as high as a state of the art GCHP system, operating at SPF = 4.0⋯4.5, but its performance is little affected by operating conditions during the investigated period.

4. Conclusions

Investigations conducted for this study lead to enhanced detailed knowledge about desiccant assisted air conditioning in winter. The main results can be summarized as follows:

- The presented system is capable of providing highly comfortable indoor air conditions during winter.
- Even though adiabatic humidification can be beneficial against enthalpy recovery, from a hygienic point of view, desiccant assisted humidification is advantageous compared to other humidification processes.
- In the context of full year operation, the significant energetic advantages of desiccant assisted air conditioning against conventional processes during dehumidification mode in summer have to be taken into account. If a desiccant assisted system is operated to make use of these advantages during summer operation, additional equipment for air humidification during winter is not required, whereas conventional air conditioning systems require additional technical equipment for air humidification.
- In combination with a ground-coupled heat pump the geothermal system can be operated efficiently as renewable heat source. Thermal energy balance of the soil is equalized throughout full year operation. Nevertheless, regarding large geothermal systems, a monitoring system is required to control and regulate input and output of thermal energy to ensure an equalized annual energy balance of the soil to run the geothermal system efficiently for long-term periods.
- In terms of further system evaluation other desiccant materials and system configuration will be taken into account experimentally as well as numerically using Modelica® system simulation models. In addition to energetic evaluations as shown in this study, a detailed economic system analysis is required for future research work.

Acknowledgement

This work is being conducted in the frame of a project funded by the Federal Ministry for Economic Affairs and Energy (German: Bundesministerium für Wirtschaft und Energie) (www.bmwi.de), cf. project funding reference number 03ET1421A.

References

[1] L.W. Davis, P.J. Gertler, Contribution of air conditioning adoption to future energy use under global warming, P. Natl. Acad. Sci. 112 (19) (2015) 5962–5967, https://doi.org/10.1073/pnas.1423558112.
[2] International Energy Agency, The Future of Cooling – Opportunities for energy-efficient air conditioning, 2018 (accessed 20 March 2019). < https://webstore.iea.org/the-future-of-cooling > .
[3] M. Isaac, D.P. van Vuuren, Modeling global residential sector energy demand for heating and air conditioning in the context of climate change, Energ. Pol. 37 (2009) 507–521, https://doi.org/10.1016/j.enpol.2008.09.051.
[4] K.F. Fong, C.K. Lee, T.T. Chow, A.M.L. Fong, Investigation on solar hybrid desiccant

cooling system for commercial premises with high latent cooling load in subtropical Hong Kong, Appl. Therm. Eng. 31 (2011) 3393–3401, https://doi.org/10.1016/j.applthermaleng.2011.06.024.
[5] P. Mazzei, F. Minichiello, D. Palma, Desiccant HVAC systems for commercial buildings, Appl. Therm. Eng. 22 (2002) 545–560, https://doi.org/10.1016/S1359-4311(01)00096-5.
[6] G. Angrisani, C. Roselli, M. Sasso, Experimental assessment of the energy performance of a hybrid desiccant cooling system and comparison with other air-conditioning technologies, Appl. Energ. 138 (2015) 533–545, https://doi.org/10.1016/j.apenergy.2014.10.065.
[7] A. Speerforck, G. Schmitz, Experimental investigation of a ground-coupled desiccant assisted air conditioning system, Appl. Energ. 181 (2016) 575–585, https://doi.org/10.1016/j.apenergy.2016.08.036.
[8] A. Speerforck, Investigation of a Desiccant Assisted Geothermal Air Conditioning System, first ed., Verlag Dr. Hut, Munich, Germany, 2019.
[9] P.L. Dhar, S.K. Singh, Studies on desiccant based hybrid air-conditioning systems, Appl. Therm. Eng. 21 (2001) 119–134, https://doi.org/10.1016/S1359-4311(00)00035-1.
[10] W. El-Maghlany, A.A. El Hefni, M. El Helw, A. Attia, Novel air conditioning system configuration combining sensible and desiccant enthalpy wheels, Appl. Therm. Eng. 127 (2017) 1–15, https://doi.org/10.1016/j.appl-thermaleng.2017.08.020.
[11] S. De Antonellis, M. Intini, C.M. Joppolo, L. Molinaroli, F. Romano, Desiccant wheels for air humidification: an experimental and numerical analysis, Energy Convers. Manage. 106 (2015) 355–364, https://doi.org/10.1016/j.enconman.2015.09.034.
[12] K. Kawamoto, W. Cho, H. Kohno, M. Koganei, R. Ooka, S. Kato, Field study on humidification performance of a desiccant air-conditioning system combined with a heat pump, Energies 9 (89) (2016) 1–22, https://doi.org/10.3390/en9020089.
[13] D. La, Y. Dai, H. Li, Y. Li, J.K. Kiplagat, R. Wang, Experimental investigation and theoretical analysis of solar heating and humidification system with desiccant rotor, Energ. Build. 43 (2011) 1113–1122, https://doi.org/10.1016/j.enbuild.2010.08.006.
[14] H. Li, Y.L. Dai, Y. Li, D. La, R.Z. Wang, Experimental investigation on a one-rotor two-stage desiccant cooling/heating system driven by solar air collectors, Appl. Therm. Eng. 31 (2011) 3677–3683, https://doi.org/10.1016/j.applthermaleng.2011.01.018.
[15] A. Preisler, M. Brychta, High potential of full year operation with solar driven desiccant evaporative cooling systems, Energ. Proc. 30 (2012) 668–675, https://doi.org/10.1016/j.egypro.2012.11.076.
[16] Y. Zhao, H. Sun, D. Tu, Effect of mechanical ventilation and natural ventilation on indoor climates in Urumqi residential buildings, Build. Environ. 144 (2018) 108–118, https://doi.org/10.1016/j.buildenv.2018.08.021.
[17] J.H. Hemmes, K.C. Winkler, S.M. Kool, Virus survival as a seasonal factor in influenza and poliomyelitis, Nature 188 (1960) 430–431.
[18] P. Fontanari, H. Burnet, M.C. Zattara-Hartmann, Y. Jammes, Changes in airway resistance induced by nasal inhalation of cold dry, dry, or moist air in normal individuals, J. Appl. Physiol. 81 (4) (1996) 1739–1743, https://doi.org/10.1152/jappl.1996.81.4.1739.
[19] W. Yang, L.C. Marr, Dynamics of airborne influenza a viruses indoors and dependence on humidity, Plos One 6 (6) (2011) 1–10, https://doi.org/10.1371/journal.pone.0021481.
[20] J.D. Noti, F.M. Blachere, C.M. McMillen, W.G. Lindsley, M.L. Kashon, D.R. Slaugther, D.H. Beezhold, High humidity leads to loss of infectious influenza virus from simulated coughs, Plos One 8 (2) (2013) 1–8, https://doi.org/10.1371/journal.pone.0057485.
[21] P. Wolkoff, The mystery of dry indoor air – an overview, Environ. Int. 121 (2018) 1058–1065, https://doi.org/10.1016/j.envint.2018.10.053.
[22] L.G. Berglund, Comfort and humidity, Ashrae Tran. 40 (1998) 35–41.
[23] L.M. Reinikainen, J.J.K. Jaakola, O. Seppänen, The effect of air humidification on symptoms and perception of indoor air quality in office workers: a six-period cross-over trail, Arch. Environ. Health 47 (1) (1992) 8–15, https://doi.org/10.1080/00039896.1992.9935938.
[24] L.M. Reinikainen, J.J.K. Jaakola, Significance of humidity and temperature on skin and upper airway symptoms, Indoor Air 13 (4) (2003) 344–352, https://doi.org/10.1111/j.1600-0668.2003.00155.x.
[25] A. Speerforck, J. Ling, V. Aute, R. Radermacher, G. Schmitz, Modeling and simulation of a desiccant assisted solar and geothermal air conditioning system, Energy 141 (2017) 2321–2336, https://doi.org/10.1016/j.energy.2017.11.151.
[26] S. J. Slayzak, J. P. Ryan, Desiccant Dehumidification Wheel Test Guide: Technical Report, NREL/TP-550-26131, 2000. Golden, National Renewable Energy Laboratory.
[27] S. De Antonellis, M. Intini, C.M. Joppolo, F. Pedranzini, Experimental analysis and practical effectiveness correlations of enthalpy wheels, Energ. Build. 84 (2014) 316–323, https://doi.org/10.016/j.en-build.2014.08.001.
[28] DIN EN 15251, Indoor environmental input for design and assessment of energy performance of buildings addressing indoor air quality, thermal environment, lightning and acoustics, 2007. Berlin, Germany: Beuth.
[29] O. Strindehag, I. Josefsson, Emission of bacteria from air humidifiers, Env. Internatl. 17 (1991) 235–241.